A. Zanotti, D. Grassi, G. Gibertini
Experimental Investigation of a Trailing Edge L-shaped Tab on a Pitching Airfoil in Deep Dynamic Stall Conditions
Proceedings of the Institution of Mechanical Engineers, Part G: Journal of Aerospace Engineering, Vol. 228, N. 12, 2014, p. 2371-2382
doi:10.1177/0954410013517089

EXPERIMENTAL INVESTIGATION OF A TRAILING EDGE L-SHAPED TAB ON A PITCHING AIRFOIL IN DEEP DYNAMIC STALL CONDITIONS

A.Zanotti[1], D.Grassi[1] and G.Gibertini[1]

1. Politecnico di Milano, Dipartimento di Scienze e Tecnologie Aerospaziali
Campus Bovisa, Via La Masa 34, 20156 Milano, Italy

Abstract: An L-shaped tab was tested at the trailing edge of an oscillating airfoil to evaluate its effects on blades aerodynamic performance. The tests were conducted on a NACA 23012 pitching airfoil in deep dynamic stall conditions with the L-shaped tab fixed in two different positions. When deployed the tab is attached to the airfoil upper surface so that the end prong protrudes at the airfoil trailing edge. In retracted position the tab features an angle of 9.1° with the airfoil upper surface, since its prong tip touches the airfoil trailing edge. The airloads time histories during a pitching cycle were measured by pressure measurements carried out on the airfoil midspan contour. The phase-averaged flow field at the trailing edge region was investigated by means of Particle Image Velocimetry to evaluate the detailed flow physics involved in the use of the device.
The experimental results indicate that the use of such a pivoting L-shaped tab can introduce similar effects to those that can be obtained by the use of an active Gurney flap. Thus, the L-shaped tab can be considered an attractive device due to its easier integration on helicopter blades.

Keywords: Oscillating airfoil, Unsteady aerodynamics, Gurney Flap, Particle Image Velocimetry.

1 INTRODUCTION

The design of new blade concepts equipped with active or passive devices has become in the recent years one of the most challenging activities in rotorcraft research environment. Many attractive solutions for improving the helicopter performance and alleviate the detrimental effects of dynamic stall [1] were investigated as, for instance, the use of air-jet vortex generators [2, 3], plasma actuators [4] or trailing edge flaps [5].

Among these studies, the interest about the effects of a Gurney flap [6] on rotor blades [7] has recently grown, as demonstrated by the several works about the study of the potential effect of an active deployable Gurney flap (see, for instance, [8, 9, 10]). Both experimental and numerical activities agree about the fact that the lift enhancement mechanism of a Gurney flap can be useful to improve the blade performance [11, 12]. In

fact, numerical studies report that benefits for rotorcraft performance can be obtained by the use of an active Gurney flap deployed on the retreating side of rotor disk and retracted on the advancing side [8, 10]. The considerations about Gurney flap control sustained by the numerical results are confirmed by wind tunnel tests carried out on a oscillating blade section model equipped with a fixed Gurney flap at the airfoil trailing edge [13].

Nevertheless, the integration of an active Gurney flap on a rotor blade represents a very challenging and costly activity, primarily due to the very severe requirement to stow the deployable device together with the required actuation mechanism inside the airfoil at the blade trailing edge. An L-shaped pivoting tab exhibits the possibility to be integrated more easily at the trailing edge region of a blade. Therefore, the main goal of the present work was to show that a pivoting L-shaped trailing edge tab can introduce effects on the blade aerodynamic performance similar to the ones that can be obtained by a deployable Gurney flap.

With this aim, an L-shaped tab was tested mounted in two different fixed positions (deployed and retracted) on a NACA 23012 blade section model oscillating in deep dynamic stall conditions [1]. The lift and pitching moment time histories were evaluated by the integration of pressure measurements carried out on the model midspan contour. The effects on the airfoil performance due to the L-shaped tab were evaluated by the comparison of the airloads curves in the different configurations tested. Moreover, the flow physics related to the use of the L-shaped tab was investigated by 2D PIV surveys carried out at the trailing edge region.

2 EXPERIMENTAL SET UP

2.1 Wind tunnel and blade section model

The experimental activity on the pitching NACA 23012 blade section model was conducted at Politecnico di Milano in the low-speed closed-return wind tunnel of the Aerodynamics Laboratory of the Dipartimento di Scienze e Tecnologie Aerospaziali (DSTA). The wind tunnel has a rectangular test section with 1.5 m height and 1 m width. The maximum wind velocity is 55 m/s and the free stream turbulence level is less than 0.1%.

The NACA 23012 airfoil was selected since, being a typical helicopter blade airfoil, it was object of experimental investigation about the fine details of dynamic stall process [14, 15, 16, 17]. The blade section model, with a $c = 0.3$ m chord and a $b = 0.93$ m span, is composed by three aluminium machined section attached to an internal metallic structure. The model central section is interchangeable depending on the measurement technique involved. In particular, one central section is equipped with 21 pressure taps positioned along the midspan airfoil contour. A different central section without taps is used to perform PIV surveys in the model midspan plane. The model is pivoted about two external steel shafts with axis at 25% c.

The layout of the experimental rig designed for testing pitching airfoils is illustrated in Fig. 1. The blade section model is mechanically jointed to a driving system that makes it to oscillate in pitch. The oscillating model driving system is composed by a brushless servomotor with a 12:1 gear drive. Two different encoders mounted on the model external shaft not joined to the motorized strut were used for feedback control and to get the instantaneous position of the model during the tests. The model pitching motion is controlled by means of an apposite code implementing a proportional and derivative control. More details about the pitching airfoil experimental rig can be found in [18, 19].

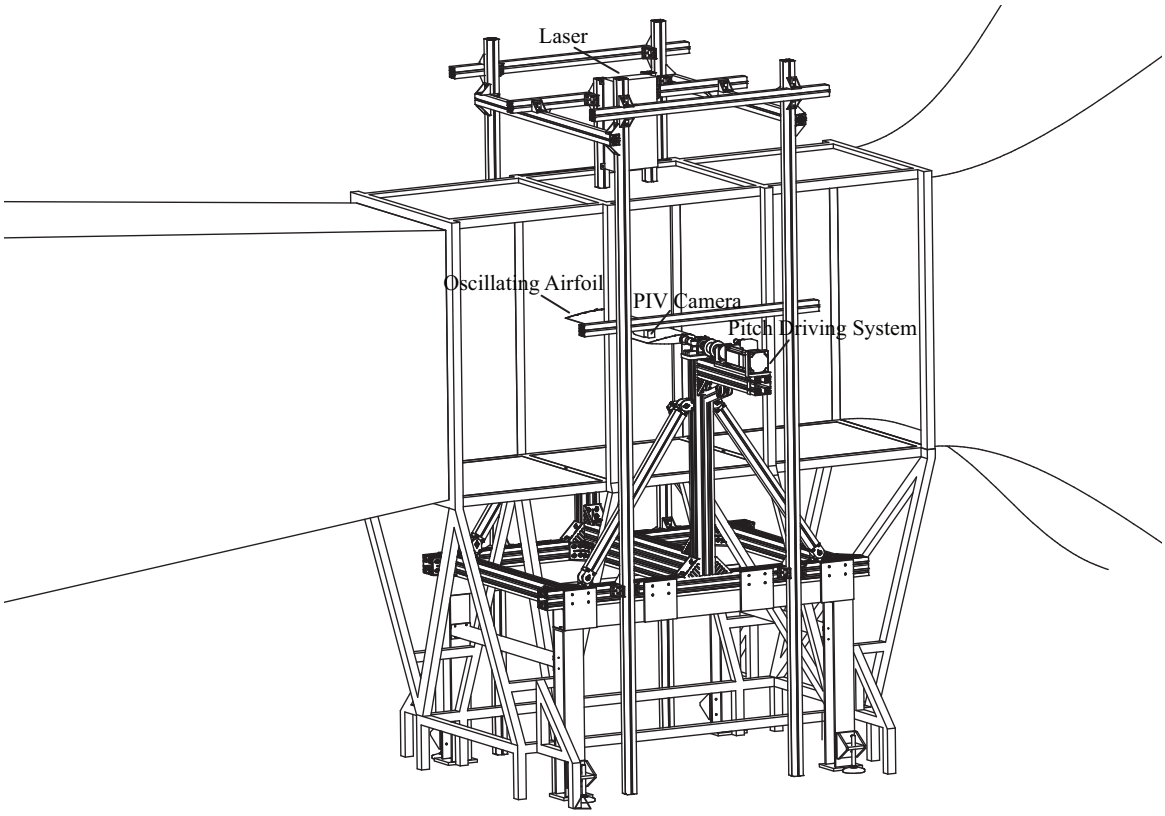

Figure 1: Layout of the experimental rig for pitching airfoils tests (PIV set up included).

2.2 Unsteady pressure measurement set up

The midspan section of the model is instrumented with 21 Kulite miniature fast-response pressure transducers. The locations of the pressure taps around the model midspan airfoil contour are illustrated in the sketch of Fig. 2.

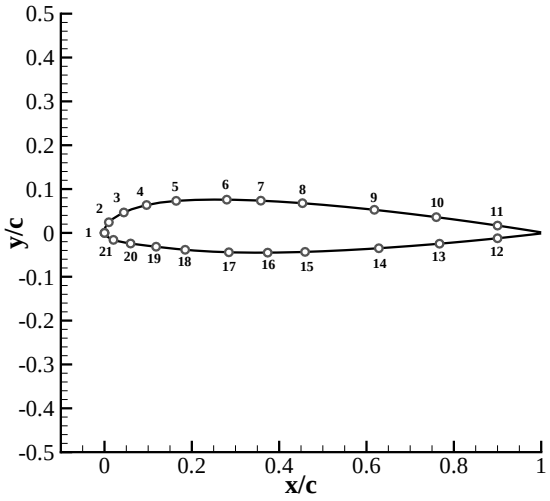

Figure 2: Pressure taps location on the NACA 23012 model midspan section.

The last pressure port on the lower and upper surfaces of the airfoil is located at 90% of the chord (similarly to the model used by Chandrasekhara et al. [13, 20]) due to feasibility problems related to probe installation at trailing edge. The time histories of the lift and pitching moment during a cycle were evaluated by the integration of the phase averaged measured pressures. The phase average of the pressure signals was computed using a bin of 0.1° angle of attack amplitude. Two second order polynomial functions interpolating the last three pressure ports signals, respectively on the upper and lower surface of the airfoil, were considered to calculate the airfoil trailing edge pressure to close the integration in chord. This pressure was calculated as the mean of the functions values extrapolated at the airfoil trailing edge position [13]. An estimation of the uncertainty due to the limited number of pressure sensors was carried out on the base of steady state simulations for clean airfoil conditions (using XFOIL code [21]). The results of this check show a maximum discretisation error in the lift and pitching moment coefficients respectively of 0.021 and 0.002 for $\alpha < 10°$. When boundary layer separation is present and particularly when the L-shaped tab is applied on the airfoil, in principle, a possible local perturbation of the pressure distribution could be introduced. Thus, a certain degree of uncertainty related to the lack of the local pressure information at the trailing edge is present and difficult to be quantified precisely. Nevertheless, the regular behaviour of the pressure up to 90% of the chord as well as the apparently rather smooth velocity field measured at the trailing edge region allowed to assume that remarkable errors are not involved in the evaluation of the global moment coefficients.

The pressure transducers signals were acquired by a National Instrument compact data acquisition system

equipped with six 24 bit A/D simultaneous bridge modules with 4 channels each. The pressure data from the transducers were collected over 30 complete pitching cycles with a sampling rate of 50 kHz.

2.3 Particle Image Velocimetry set up

A double shutter CCD camera with a 12 bit, 1952×1112 pixel array equipped with a 55 mm lens was used to get the image pairs. The 2D PIV surveys were carried out with a measurement window covering the trailing edge region where the L-shaped tab is installed. The PIV system used a Nd:Yag double pulsed laser with 200 mJ output energy and a wavelength of 532 nm. The laser sheet passed through an opening in the wind tunnel roof aligned with the flow and positioned at the midspan of the test section width. The camera line of sight was perpendicular to the laser sheet during the tests. The laser and the camera were mounted on a external metallic structure made of aluminium profiles. The metallic structure is connected to a heavy basement in order to avoid during the tests the transfer of the wind tunnel vibrations to the PIV measurement devices(see Fig. 1). A particle generator with Laskin nozzles was used for the flow seeding. The tracer particles, consisting in small oil droplets with a diameter within the range of 1-2 μm, were injected in correspondence of a section just after the fans till the wind tunnel volume was fullfilled with homogeneous density. The image pairs post-processing was carried out using the PIVview 2C software [22] of PIVTEC. Multigrid technique [23] was employed to correlate the image pairs, up to an interrogation window of 16×16 pixels. The velocity flow fields were phase averaged over 100 image pairs.

2.4 L-shaped tab

For the present activity an L-shaped tab was manufactured using two carbon fiber skins. The tab is 0.5 mm thick and it spans the entire blade section model with a 25 mm chord. The L-shaped tab was attached on the model upper surface at the trailing edge region and it was tested in the two fixed positions illustrated in Fig. 3.

When deployed, as shown in Fig. 3a, the tab is flush with the airfoil upper surface. Thus, the end prong of the tab is not a Gurney flap according to the definition of Liebeck [6], as it is perpendicular to the airfoil upper surface. In this configuration the end prong of the tab protrudes 4 mm from the trailing edge (3.95 mm in vertical direction) corresponding to 1.3% c of effective height. The end prong features respectively an angle of 74.46° (see Fig. 4) with the airfoil lower surface and an angle of 81.2° with the chord direction. Due to the moderate deviation from the 90° mounting angle, a behaviour similar to a classic Gurney flap is expectable. This consideration is supported by the results of Li et al. [24] showing that the effects of a 90° and a 135° flap are apparently similar.

A particular of the L-shaped tab mounted on the blade section model in deployed position can be observed

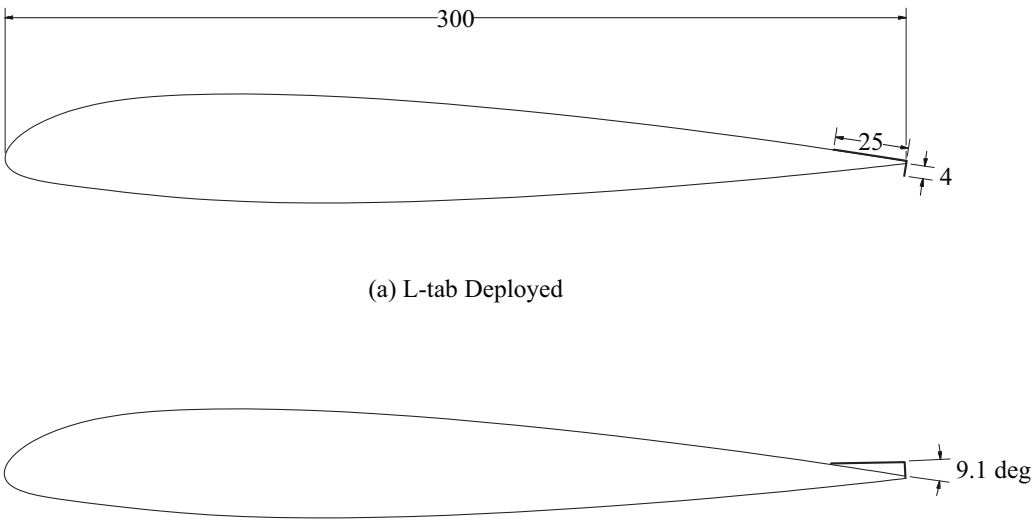

Figure 3: L-shaped tab layout at the NACA 23012 airfoil trailing edge (dimensions in mm).

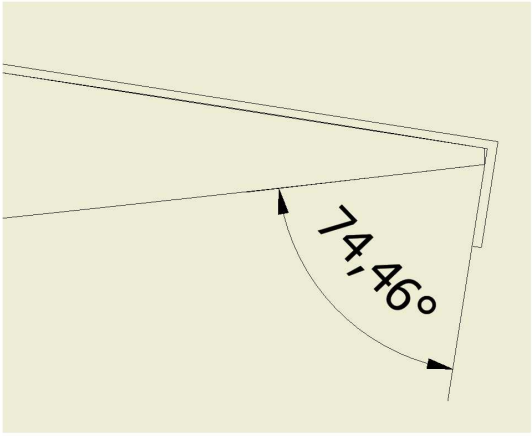

Figure 4: Detail of the trailing edge with L-shaped tab deployed.

in Fig. 5.

When retracted as shown in Fig. 3b, the L-shaped tab features an angle 9.1° with the airfoil upper surface, since the prong tip touches the trailing edge.

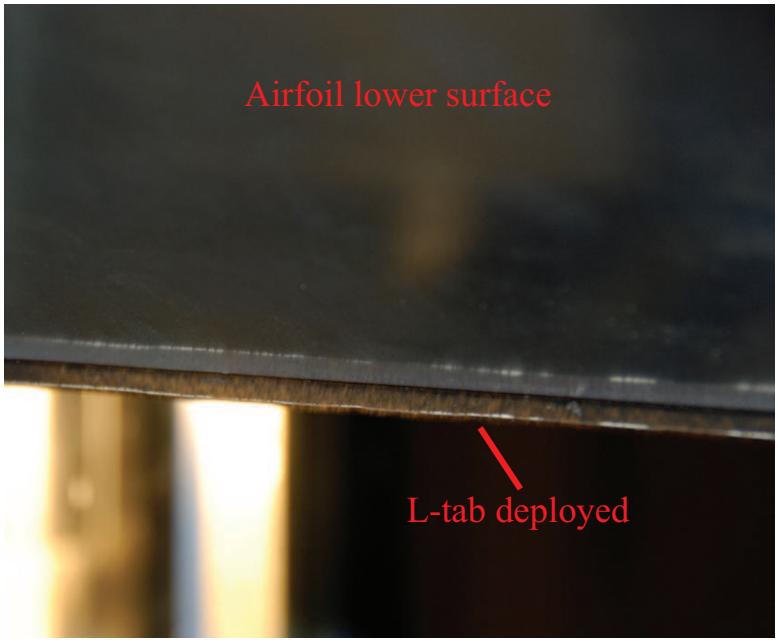

Figure 5: Particular of the L-shaped tab mounted on the blade section model in deployed position.

3 RESULTS AND DISCUSSION

The L-shaped tab was tested in two deep dynamic stall conditions, consisting in a sinusoidal pitching cycle characterised by a mean angle of attack of $\alpha_m = 10°$ and 15°, respectively, with constant oscillation amplitude of $\alpha_a = 10°$ and reduced frequency $k = 0.1$. The tests were carried out at $U_\infty = 30$ m/s, corresponding to Re $= 6 \times 10^5$ and M $= 0.09$. The Reynolds number representative of a small-medium size helicopter retreating rotor blade section at about 65% radius in forward flight should be of the order of $1 \cdot 10^6$ ($M = 0.15$). In the present test activity a lower testing speed was chosen to avoid fatigue issues on the model strut. Nevertheless, the Reynolds number of the present tests is not far from a real flight condition. Consequently the effects due to the L-shaped tab are expected to be similar, as the boundary layer thickness can be considered comparable. On the other hand, the reproduced reduced frequency is representative of a real flight condition.

Pressure measurements and PIV surveys were not done simultaneously. The different measurement techniques were carried out during dedicated wind tunnel runs using the model midspan sections previously described. This solution was preferred in order to protect the transducers sensors from the oil seeding and the laser light.

An assessment of the test repeatability is presented in Fig. 6 showing the phase averaged airloads coefficients curves evaluated for the clean airfoil configuration in two different wind tunnel runs. A quite good repeatability

of the tests can be observed during all the pitching cycle. Small discrepancies between the pitching moment curves can be observed just in the range between $16° < \alpha < 18°$ in downstroke. In fact, the flow field in this incidence range is characterised by severe unsteadinees, as it was shown in the works by Zanotti and Gibertini [15] and Zanotti et al. [16].

Figurer 7 and 8 show the comparison of the lift and quarter chord moment coefficients evaluated with the L-shaped tab deployed and retracted with respect to the clean airfoil configuration. The standard deviation of the airloads coefficients are plotted on all the airloads coefficients curves.

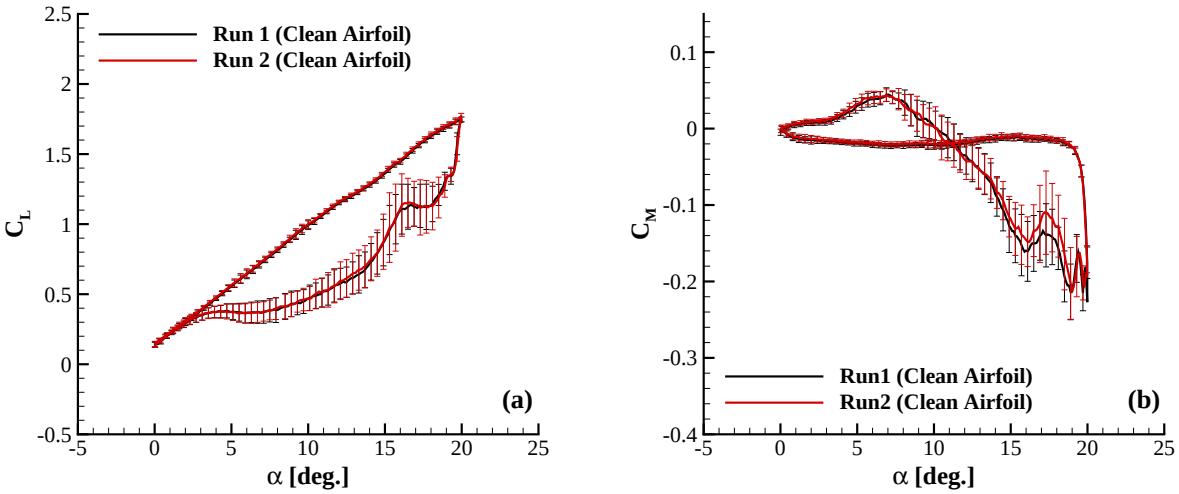

Figure 6: Test repeatability of the airloads curves measured for $\alpha = 10° + 10° \sin(\omega t)$, $k = 0.1$ (Re $= 6 \times 10^5$ and M $= 0.09$).

The test results show that the deployed L-shaped tab introduces remarkable effects on the airloads curves. In fact, the measured lift and pitching moment curves are shifted with respect to the clean airfoil configuration. In particular, the deployed L-shaped tab behaves similarly to a Gurney flap, as it generates in upstroke a larger lift with respect to the clean airfoil configuration for both the pitching conditions tested. The observed increase of the lift coefficient occurring when the L-shaped tab is deployed can be very useful in upstroke motion due to an associated higher level of available thrust for the retreating blade.

The pitching moment curves comparison shows that the deployed L-shaped tab introduces a more severe C_M peak at the stall incidence. These results are qualitatively in agreement with the experimental results obtained by Chandrasekhara et al. [13] for a pitching VR-12 airfoil equipped with a Gurney flap at the trailing edge. A direct comparison is not presented as these data were obtained for a different airfoil and a different Mach

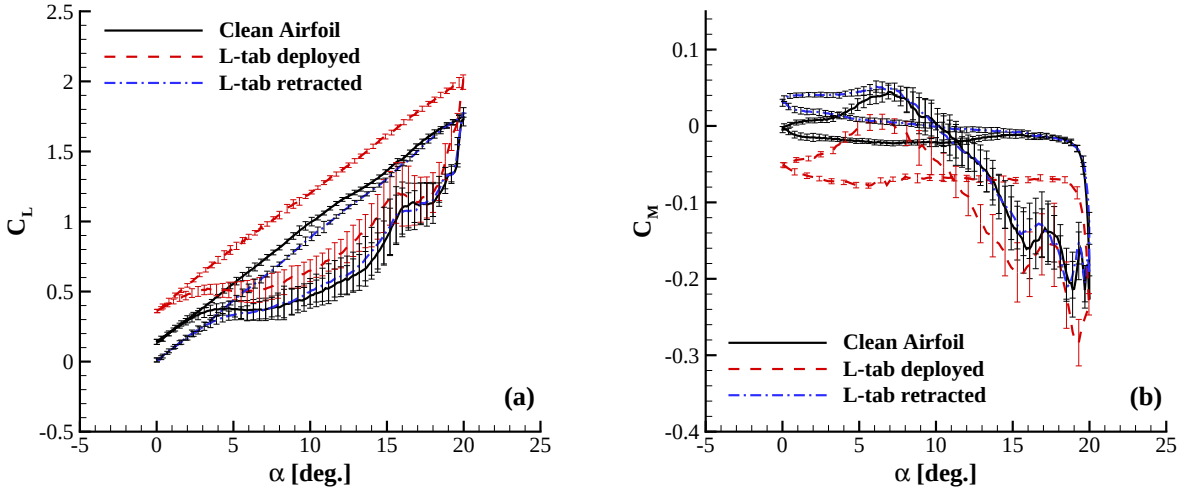

Figure 7: Comparison of the airloads curves measured for $\alpha = 10° + 10° \sin(\omega t)$, $k = 0.1$ (Re $= 6 \times 10^5$ and M $= 0.09$).

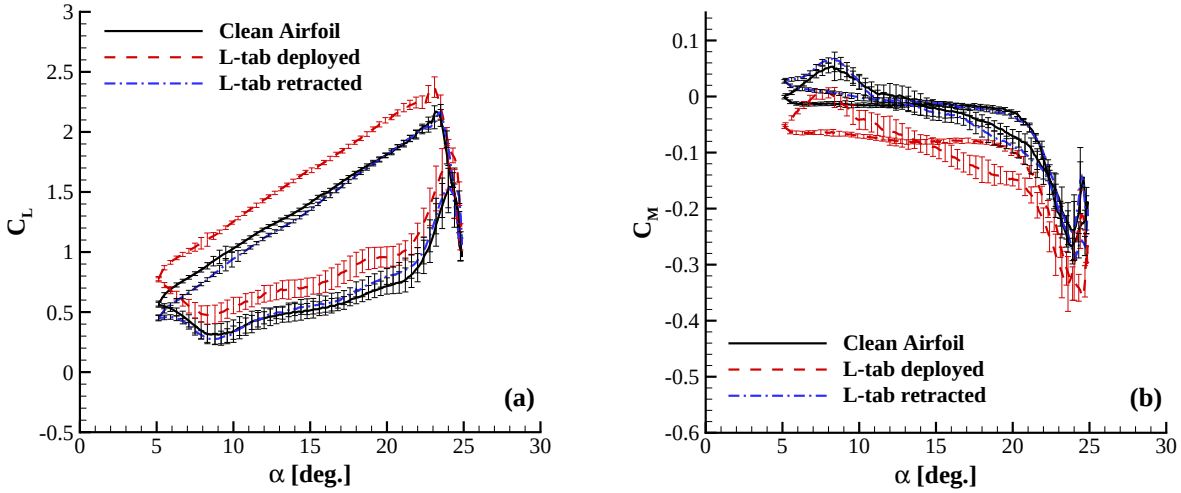

Figure 8: Comparison of the airloads curves measured for $\alpha = 15° + 10° \sin(\omega t)$, $k = 0.1$ (Re $= 6 \times 10^5$ and M $= 0.09$).

number.

The results obtained with the retracted L-shaped tab show smaller differences with respect to the clean

configuration, mainly in the low incidence part of the pitching cycle, indicating that the tab behaves like a slightly upward deflected flap. The pitching moment curves comparison shows that the retracted L-shaped tab does not introduce penalties concerning the C_M peak, as for both the tested conditions the measured C_M peaks are comparable to the ones obtained for the clean case.

The effects of the L-shaped tab on the aerodynamic damping were investigated by the evaluation of the Liiva damping coefficients defined as the ratio between the closed-loop integral of the measured C_M and the theoretical value derived from Theodorsen's theory [25, 26, 27]. Indeed, a net positive aerodynamic damping can be considered an important benefit for a rotor blade, as it would avoid the risk of stall flutter occurrence [28]. The damping coefficients calculated for all the configurations tested are reported in Tab. 1.

	Clean	**L-tab deployed**	**L-tab retracted**	**with ideal control**
$\alpha(t) = 10° + 10° \sin(\omega t)$	-0.548	-0.384	-0.734	0.915
$\alpha(t) = 15° + 10° \sin(\omega t)$	0.202	0.028	-0.05	1.538

Table 1: Liiva damping coefficients [25] evaluated for the different L-shaped tab configurations tested and for an ideal control law.

For the test condition with $\alpha_m = 10°$ the net aerodynamic damping is negative for the clean airfoil and both the configurations with the L-shaped tab (see Tab. 1). On the other hand, for the test condition with $\alpha_m = 15°$ the net aerodynamic damping is positive for the clean airfoil and for the configuration with the L-shaped tab deployed, while a quite small negative value of the damping coefficient was evaluated for the retracted L-shaped tab configuration (see Tab. 1). However, the behavior of the C_M curves measured for the different tested configurations suggests an ideal potential control law for an active pivoting L-shaped tab. In fact, deploying the L-shaped tab during the upstroke motion and retracting the tab during the downstroke increases the C_M curve counterclockwise loop area associated to a positive aerodynamic damping and reduces the clockwise loop area associated to a negative aerodynamic damping. This consideration is supported by the positive values of the damping coefficients calculated considering the C_M curve measured with the deployed L-shaped tab in the upstroke phase of the pitching cycles and the one measured with the retracted tab in the downstroke phase up to close the loop (see the results reported in the fifth column of Tab. 1). Nevertheless, it has to be specified that the values of the aerodynamic damping coefficients calculated with this potential control law represents an ideal estimation of the maximum effects on damping obtainable with such an active controlled device. These values were obtained assuming an instantaneous switch from the deployed tab curve to the retracted one and viceversa.

In fact, the scope of the present paper was not to specify the details of the control law of the L-shaped tab,

as an active control system to drive this device was not available in the present test set up. However, the ideal potential control law described in the previous discussion is in line with the one suggested by the results of the numerical simulations carried out by Yeo [8] on a deployable Gurney flap.

The stronger lift breakdown and the more severe C_M peak that would be introduced at stall by the deployed L-shaped tab should be probably avoided retracting the tab before the end of the upstroke motion, just before the stall onset. Of course, a decrease of the benefit in damping would be associated to this feature.

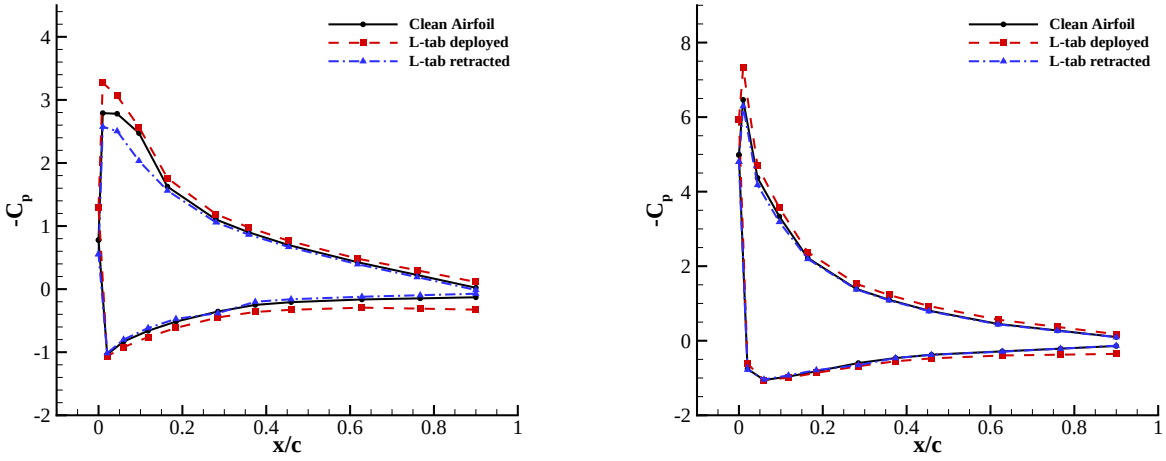

(a) $\alpha = 12°$ upstroke

(b) $\alpha = 18°$ upstroke

Figure 9: Comparison of the pressure coefficient distributions measured for $\alpha = 10° + 10° \sin(\omega t)$, $k = 0.1$.

More details about the effects introduced by the L-shaped tab during the upstroke motion can be deduced from the comparison of the pressure coefficient distributions. Figures 9a and b show respectively the comparison of the $-C_p$ distributions measured at $\alpha = 12°$ and $18°$ in upstroke for the test condition with $\alpha_m = 10°$.

The lift increase introduced deploying the L-shaped tab is due to both a higher suction (lower pressure) on the upper surface and to a higher pressure on the lower surface (particularly at the trailing edge region). These effects are typically produced by Gurney flaps and they are often explained by the modification of the Kutta condition [13] due to the vortex structure behind the Gurney flap itself. The local pressure increase at lower surface trailing edge is due the flow slowing down at the forward facing side of the tab prong.

The $-C_p$ distribution behavior measured with the the L-shaped tab retracted is very close to the clean airfoil pressure distribution for $\alpha = 18°$, showing that retracting the L-shaped tab does not introduce remarkable effects upstream this device at this angle of attack. On the other hand, for a lower angle of attack $\alpha = 12°$, where a lift difference with respect to the clean airfoil configuration occurs, the behaviour of the $-C_p$ distribution measured

with the L-shaped tab retracted shows a lower suction at the leading edge region.

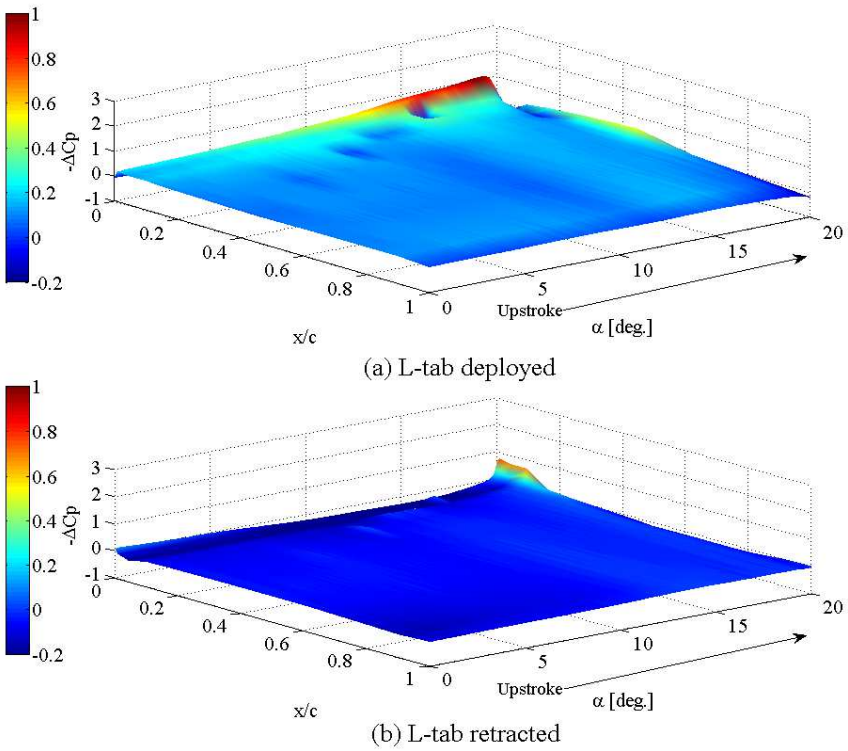

Figure 10: ΔC_p distribution evaluated on the airfoil upper surface in upstroke for $\alpha = 10° + 10° \sin(\omega t)$, $k = 0.1$.

Figure 10 shows the distribution of the pressure coefficient difference with respect to the clean airfoil configuration (ΔC_p) evaluated on the airfoil upper surface during the upstroke motion for the test condition with $\alpha_m = 10°$. The ΔC_p distribution measured with the L-shaped tab deployed shows that the peak pressures over the airfoil upper surface are higher with respect to the clean airfoil and spread over a large angles of attack range in upstroke (see Fig. 10a). This feature leads to the production of the sensible higher lift level observed in Fig. 7a.

On the other hand, Figure 10b shows that the pressure distribution measured on the airfoil upper surface with the L-shaped tab retracted retraces rather the clean airfoil distribution for almost all the upstroke motion, with a small difference just at the stall onset.

The discussion about the effects of the L-shaped tab on the blade performance should be completed by the assessment of the drag contribution. Nevertheless, just the pressure drag contribution is available from the present measurements. The measure of the total drag for a deep dynamic stall condition represents, in fact,

a very challenging activity due to the severe unsteadiness conditions that characterise this phenomenon. The attempt to obtain the total drag by means of wake phase averaged measurements did not succeed to produce a very accurate estimation as many sources of uncertainty are present in the problem [29]. However, an indication about the drag penalty introduced by the tab can be deduced from the pressure drag contribution comparison shown in Fig. 11 for both the pitching conditions tested.

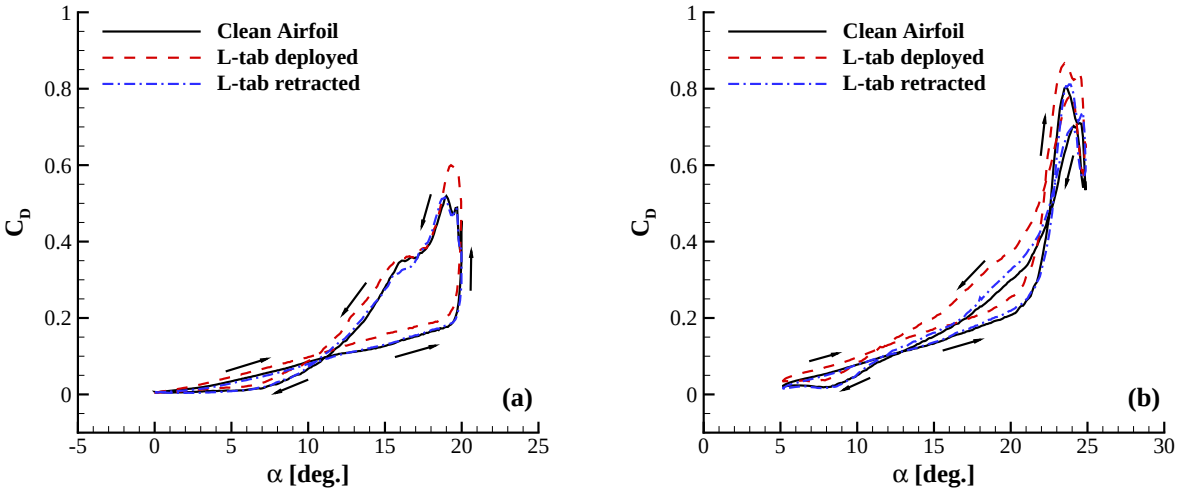

Figure 11: Comparison of the drag coefficient distribution; (a) $\alpha = 10° + 10° \sin(\omega t)$, (b) $\alpha = 15° + 10° \sin(\omega t)$.

Interestingly, the pressure drag distributions evaluated with the L-shaped tab present not remarkable differences with respect to the clean airfoil configuration one. In particular, it can be just observed that the L-shaped tab deployed produces a higher peak of the drag at stall incidence for both the tested conditions and a higher drag increase during the downstroke phase for the pitching condition with $\alpha_m = 15°$. Consequently, the present experimental data suggest that a contained drag penalty should be introduced by an active controlled pivoting L-shaped tab, deployed during the upstroke up to the stall onset and then retracted as long as the pitching cycle restarts. Nevertheless, information about the viscous drag contribution should be necessary to close this issue.

The influence of the L-shaped tab deployed and retracted on the flow field at the airfoil trailing edge region was investigated by means of PIV surveys carried out at $\alpha = 9°$ and $18°$ both in upstroke and downstroke for the pitching cycle condition with $\alpha_m = 10°$. In the following figures, PIV results are illustrated by means of the velocity magnitude contours and the in-plane streamlines patterns.

The instantaneous PIV measurement carried out at $\alpha = 9°$ in upstroke shows that, similarly to a Gurney flap

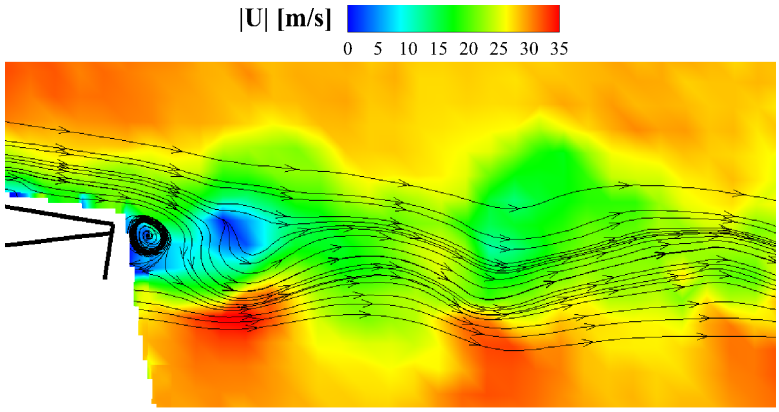

Figure 12: Particular of the instantaneous PIV flow field measured at $\alpha = 9°$ upstroke for $\alpha = 10° + 10° \sin(\omega t)$, $k = 0.1$ with the L-shaped tab deployed.

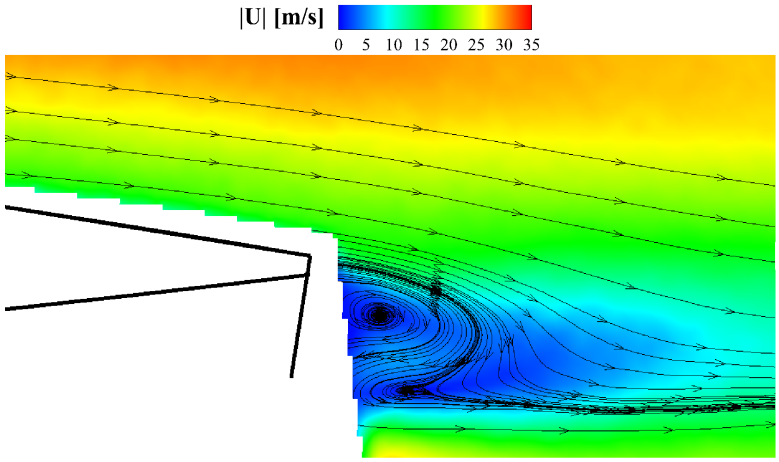

Figure 13: Particular of the phase averaged PIV flow field measured at $\alpha = 9°$ upstroke for $\alpha = 10° + 10° \sin(\omega t)$, $k = 0.1$ with the L-shaped tab deployed (interrogation window of 8×8 pixels).

case [9, 30], the flow field downstream the deployed L-shaped tab is apparently unsteady and it is characterised by a vortex street that can be observed in Fig. 12. As it can be deduced from Fig. 12, the characteristic frequency of this vortex street should be estimated of the order of few hundreds of Hz. Thus, the present PIV measurements could not resolve the time history of the wake due to the limited response in frequency of the employed instrumentation.

For the same test case, the detail of the phase averaged flow field evaluated in the wake region using a smaller minimum interrogation window of 8×8 pixels shows, behind the end prong of the tab, two counter-rotating

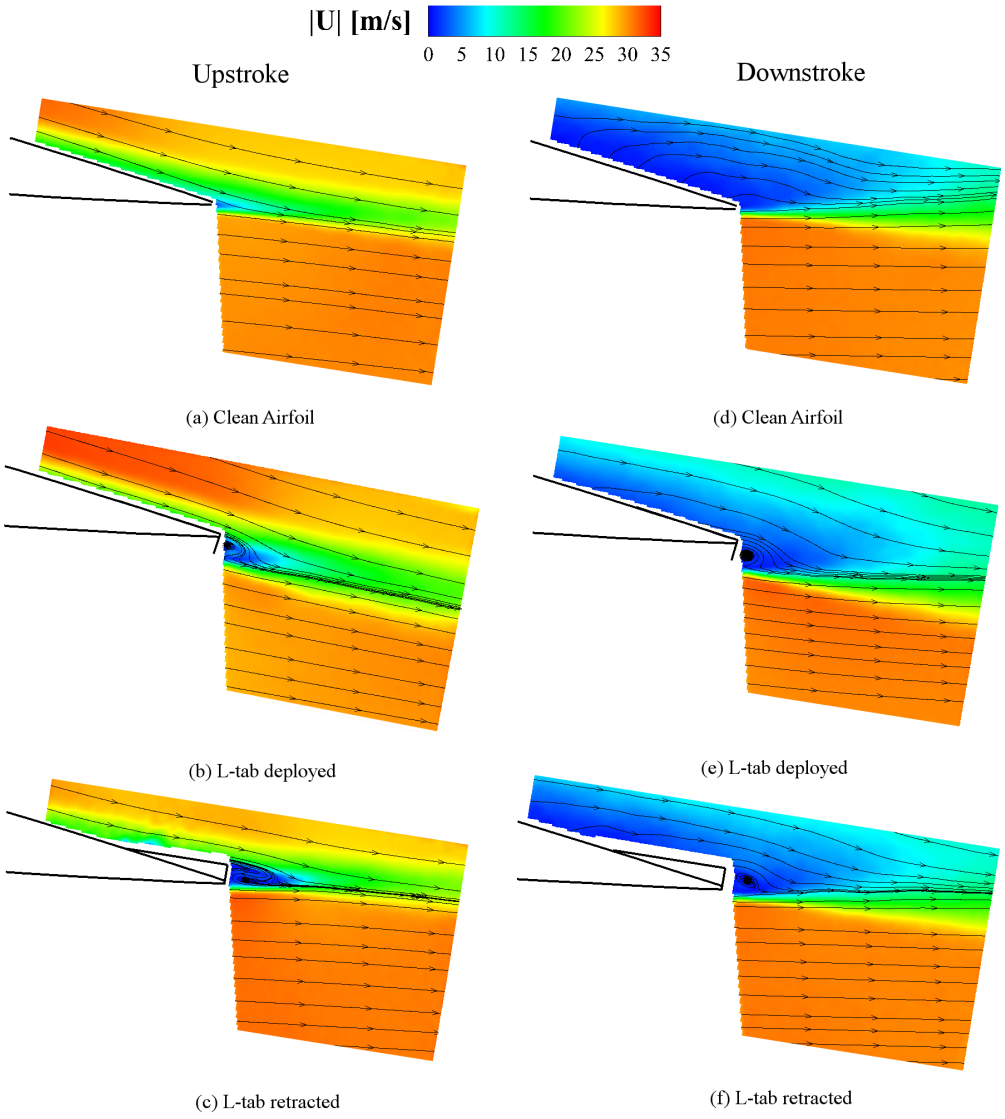

Figure 14: Comparison of the phase averaged PIV flow fields measured at $\alpha = 9°$ for $\alpha = 10° + 10° \sin(\omega t)$, $k = 0.1$ with the L-shaped tab.

vortices (see Fig. 13b). This feature is analogous to what it was found for attached flow conditions downstream of a Gurney flap [9] but with the lower cell quite smaller in the present test case.

The phase averaged overall flow fields evaluated by PIV surveys at $\alpha = 9°$ and $18°$ are shown respectively in Fig. 14 and Fig. 15. In order to reduce the noise level in these figures, it was used a minimum interrogation windows of 16×16 pixels to correlate the image pairs.

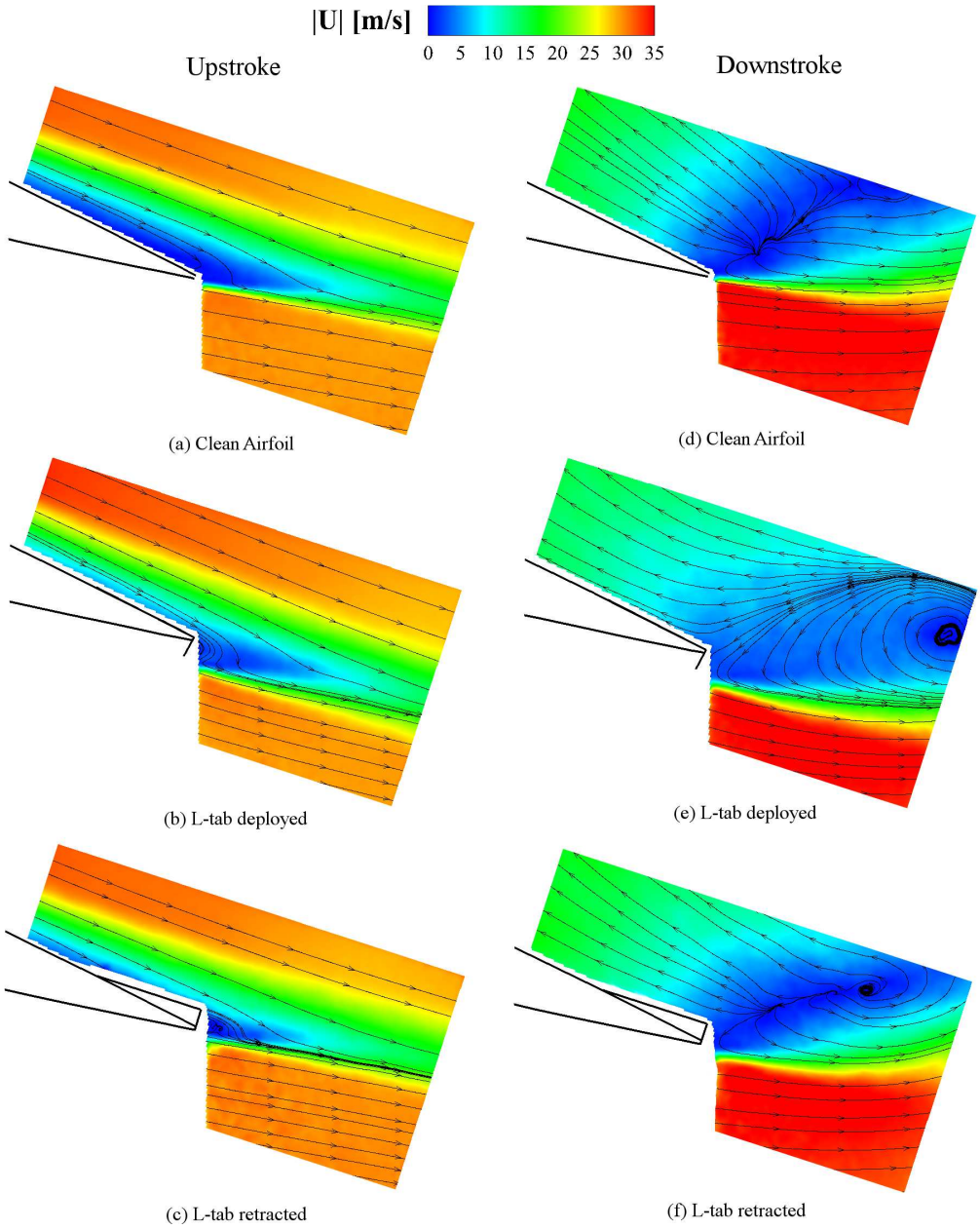

Figure 15: Comparison of the phase averaged PIV flow fields measured at $\alpha = 18°$ for $\alpha = 10° + 10° \sin(\omega t)$, $k = 0.1$ with the L-shaped tab.

At $\alpha = 9°$ in upstroke the overall flow field on the clean airfoil upper surface is completely attached, as it can be observed in Fig. 14a. When deployed the L-shaped tab behaves similarly to a Gurney flap producing

the downward deflection of the wake (see Fig. 14b).

The retracted L-shaped tab behaves as an upward deflected trailing edge flap producing the upward deflection of the wake. The flow field behind the end prong of the tab shows a structure similar to the one observed for the deployed tab test case that is characterised by a quite bigger closed cell turning counterclockwise (see Fig. 14c).

At $\alpha = 9°$ in downstroke a very low speed flow region can be observed at the trailing edge for the clean airfoil configuration (see Fig. 14d). As it is apparent in the airloads curves of Fig. 7, this condition is still stalled although no back-flow is evident. In fact, three-dimensional separation does not necessarily involve back-flow and it is tipically characterised by a remarkable stream-wise vorticity component. In particular, the perpendicular-to-surface pattern of the in-plane streamlines observed in Fig. 14d is compatible with this scenario. A contribution to the streamlines perpendicular patterns is also due to the convection produced by the airfoil motion, as the camera is not moving with the airfoil. In fact, at this angle of attack, the airfoil angular velocity is close to the maximum value reached during the pitching cycle.

At this angle of attack the main apparent features observed in the flow field when the L-shaped tab is deployed or retracted are the occurrence of a vortex structure just downstream the end prong of the tab and the reduction of the very low speed region extension with respect to the clean airfoil case (see Fig. 14e and f).

At $\alpha = 18°$ in upstroke the stall is delayed by the effect of the rapid positive pitching rate [15], then the flow field is attached on the most of the clean airfoil upper surface. Nevertheless, at this angle of attack a small separation region can be observed at the airfoil trailing edge (see Fig. 15a).

In this test condition the L-shaped tab both deployed or retracted promotes the attachment of the flow on the airfoil upper surface (see Fig. 15b and c).

At $\alpha = 18°$ in downstroke the flow on the clean airfoil upper surface presents a wide three-dimensional separation region characterised by strong vortices [16, 31]. Thus, the flow fields presented in Fig. 15 have to be taken in account just for giving an indication about the local effects introduced by the L-shaped tab, as they represents planar cuts through a strongly three-dimensional flow field.

In particular, for the clean airfoil configuration the measured flow field shows a wide reverse flow region at the trailing edge region (see Fig. 15d).

It can be seen from Fig. 15e and f) that the wake flow structure is modified by the L-shaped tab but the velocity distribution over the airfoil is only slightly affected .

4 CONCLUSIONS

An experimental campaign carried out on a pitching NACA 23012 airfoil in deep dynamic stall conditions allowed to evaluate the effects on the aerodynamic performance of a L-shaped tab positioned at the airfoil trailing edge.

The pressure measurements results demonstrated that advantages for the main rotor performance can be obtained deploying the L-shaped tab during the upstroke motion, corresponding to a conspicuous increase of the retreating blade lift. However, a stronger lift breakdown and a higher peak of the pitching moment in correspondence of the stall are observed with the L-shaped tab deployed, similarly to what it was found in literature with a Gurney flap. Retracting the tab during downstroke would reduce the risk of stall flutter occurrence. Moreover, PIV surveys were used to investigate the detailed flow physics related to the use of the L-shaped tab, in particular at the trailing edge region.

Although a qualitative control law was suggested by the experimental results, the main goal of the work was to show that the benefits for blade performance achievable with a deployable Gurney flap can be obtained by the use of a pivoting L-shaped tab. This concept device shows an easier installation on helicopter blades. In fact, the pivoting L-shaped tab can be integrated on the blade external surface, while its actuation mechanism can be stowed inside the blade upstream the trailing edge, where the space requirement are not particularly severe. Moreover, a preliminary assessment of drag based on the measure of pressure drag contribution shows that a contained drag penalty would be associated to the use of the pivoting L-shaped tab. Hence, the experimental results obtained with the fixed L-shaped tab encourage the research activity to manufacture and test this solution on a blade model.

Funding

This research received no specific grant from any funding agency in the public, commercial, or not-for-profit sectors.

APPENDIX

Nomenclature

b	blade section model span [m]
c	blade section model chord [m]
C_D	drag coefficient
C_L	lift coefficient
C_M	pitching moment coefficient about the airfoil quarter chord
C_p	pressure coefficient
DSTA	Dipartimento di Scienze e Tecnologie Aerospaziali
f	oscillation frequency [Hz]
k	reduced frequency, $\equiv \pi f c/U_\infty$
M	Mach number
PIV	Particle Image Velocimetry
Re	Reynolds number
$\|U\|$	velocity magnitude [m/s]
U_∞	free-stream velocity [m/s]
x	stream-wise coordinate [m]
α	angle of attack [deg]
α_m	mean angle of attack [deg]
α_a	pitching oscillation amplitude [deg]
ΔC_p	pressure coefficient difference with respect to clean airfoil
ω	circular frequency [rad/s]

References

[1] McCroskey WJ. The Phenomenon of Dynamic Stall. NASA TM 81264, 1981.

[2] Gardner A, Richter K, Maiand H and Neuhaus D. Experimental control of compressible oa209 dynamic stall by air jets, *38th European Rotorcraft Forum*, Amsterdam, The Netherlands, 4-7 September 2012.

[3] Singh C, Peake D, Kokkalis A, Khodagolian V, Coton F and Galbraith R. Control of Rotorcraft Retreating Blade Stall Using Air-Jet Vortex Generators. *Journal of Aircraft* 2006; 43: 1169–1176.

[4] Post M and Corke T. Separation Control Using Plasma Actuators: Dynamic Stall Vortex Control on Oscillating Airfoil. *AIAA Journal* 2006; 44: 3125–3135.

[5] Feszty D, Gillies E and Vezza M. Alleviation of Airfoil Dynamic Stall Moments via Trailing-Edge Flap Flow Control. *AIAA Journal* 2001; 42: 17–25.

[6] Liebeck RH. Design of subsonic airfoils for high lift. *Journal of Aircraft* 1978; 15: 547-561.

[7] Kentfield JAC. The potential of gurney flaps for improving the aerodynamic performance of helicopter rotors. *AIAA International Powered Lift Conference* 1993, AIAA Paper 93-4883.

[8] Yeo H. Assessment of active controls for rotor performance enhancement. *Journal of the American Helicopter Society* 2008; 53: 152-163.

[9] Kinzel MP, Maughmer MD and Duque EPN. Numerical investigation on the aerodynamics of oscillating airfoils with deployable gurney flaps. *AIAA Journal* 2010; 48: 1457-1469.

[10] Pastrikakis V, Steijl R and Barakos GN. Computational Analysis of the W3 Sokol Rotor with Gurney Flaps, *39th European Rotorcraft Forum*, Moscow, Russia, 3-6 September 2013.

[11] Maughmer MD and Bramesfeld G. Experimental investigation of gurney flaps. *Journal of Aircraft* 2008; 45: 2062-2067.

[12] Yee K, Joo W and Lee DH. Aerodynamic performance analysis of a gurney flap for rotorcraft application. *Journal of Aircraft* 2007; 44: 1003-1014.

[13] Chandrasekhara M, Martin P and Tung C. Compressible Dynamic Stall Performance of a Variable Droop Leading Edge Airfoil with a Gurney Flap. *Journal of American Helicopter Society* 2008; 53: 18–25.

[14] Leishman JG. Dynamic stall experiments on the NACA 23012 aerofoil. *Experiments in Fluids* 1990; 9: 49–58.

[15] Zanotti A and Gibertini G. Experimental investigation of the dynamic stall phenomenon on a NACA 23012 oscillating airfoil. *Proceedings of the Institution of Mechanical Engineers, Part G: Journal of Aerospace Engineering* 2013; 227: 1375–1388.

[16] Zanotti A, Melone S, Nilifard R and D'Andrea A. Experimental-numerical investigation of a pitching airfoil in deep dynamic stall, *Proceedings of the Institution of Mechanical Engineers, Part G: Journal of Aerospace Engineering*, Epub ahead of print 26 February 2013, doi:10.1177/0954410013475954.

[17] Zanotti A, Gibertini G, Grassi D and Spreafico D. Wake Measurements behind an Oscillating Airfoil in Dynamic Stall Conditions. *ISRN Aerospace Engineering* 2013, 1: 1–11.

[18] Zanotti A. Retreating Blade Dynamic Stall, Ph.D. thesis, Politecnico di Milano, 2012.

[19] Zanotti A, Auteri F, Campanardi G and Gibertini G. An Experimental Set Up for the Study of the Retreating Blade Dynamic Stall. *37th European Rotorcraft Forum*, Gallarate (VA), Italy, 13-15 September 2011.

[20] Chandrasekhara M, Martin P and Tung C. Compressible Dynamic Stall Control Using a Variable Droop Leading Edge Airfoil. *Journal of Aircraft* 2004; 41: 862-869.

[21] Drela M and Youngren H, XFOIL 6.94 User Guide, Cambridge MA, 2001.

[22] PIVview 2C version 3.0, User Manual, PIVTEC, www.pivtec.com.

[23] Raffel M, Willert C and Kompenhans J. *Particle Image Velocimetry, a practical guide*. Springer, Heidelberg, 1998.

[24] Li Y, Wang J and Zhang P. Influences of Mounting Angles and Locations on the Effects of Gurney Flaps. *Journal of Aircraft* 2003; 40: 494–498.

[25] Liiva J. Unsteady aerodynamic and stall effects on helicopter rotor blade airfoil sections. *Journal of Aircraft* 1969; 6: 46–51.

[26] Leishman JG. *Principles of helicopter aerodynamics*. Cambridge University Press, 2006.

[27] Theodorsen T, On the theory of wing sections with particular reference to the lift distribution, NACA TR 383, 1932.

[28] Carta FO. An Analysis of the Stall Flutter instability of Helicopter Rotor Blades. *Journal of American Helicopter Society* 1967; 12: 1–8.

[29] Gibertini G, Auteri F, Grassi D, Spreafico D and Zanotti A. Experimental method for drag measurement of an oscillating airfoil in dynamic stall condition. *38th European Rotorcraft Forum*, Amsterdam, The Netherlands, 4-7 September 2012.

[30] Jarkowski M, Woodgate M and Barakos GN. Comparison between Sliding and Chimera Grids. *39th European Rotorcraft Forum*, Moscow, Russia, 3-7 September 2013.

[31] Zanotti A, Nilifard R, Gibertini G, Guardone A and Quaranta G. Experimental-Numerical Investigation of the Dynamic Stall Phenomenon over the NACA 23012 Airfoil. *38th European Rotorcraft Forum*, Amsterdam, The Netherlands, 4-7 September 2012.